Journal of Structural Geology. Vol. 4, No. 4, pp. 429 to 442, 1982
Printed in Great Britain

0191-8141/82/040429-14 $03.00/0

Deformation mechanisms and flow regimes in limestones from the Helvetic zone of the Swiss Alps

O. Adrian Pfiffner

Institut de Géologie, Université de Neuchâtel, 11 rue Emile-Argand, CH-2000 Neuchâtel, Switzerland

(*Received* 4 *March* 1982; *accepted in revised form* 25 *June* 1982)

Abstract—This paper is based on a combined field, transmission-electron (TEM) and transmission-optical (TOM) microscope study of limestones from the Helvetic zone (Swiss Alps) and discusses the deformation mechanisms and flow regimes that governed the deformation of these rocks.

During pre-metamorphic regional ductile deformations the limestones deformed by power-law dislocation creep with differential stresses probably not exceeding 1 kbar. Dynamic recrystallization with grain-boundary sliding and grain-boundary migration allowed the grains to be less elliptical than the strain ellipse. A characteristic of the structure is the existence of dislocation-free subgrains. In the footwall of and approaching the Lochseiten calc-mylonite along the Glarus overthrust, grain-boundary sliding becomes more important (shift to diffusional creep or superplastic flow).

During a syn- and post-metamorphic deformation, dynamic recovery seems to have become less competitive (no dislocation-free sub-grains), and along thrust faults twinning indicates a shift to higher differential stresses at the close of the deformation.

It was not possible to separate these deformation phases on the basis of the dislocation debris. Sub-grain sizes as observed in TEM and TOM were identical.

In limestones that underwent cataclastic deformation the rocks seem to have started breaking up along the grain boundaries. The new grain fragments are very small (0.1–0.3 μm) and are heavily twinned. In TEM the old large grains show very long straight glide dislocations, cleavage and, when shattered, ring patterns in diffraction.

INTRODUCTION

The Helvetic zone of eastern Switzerland is an area that has been extensively analysed from a structural point of view. Here it is possible to sample limestones on which we have relatively good control as to their deformational and metamorphic history.

Transmission electron microscopy (TEM) has proven to be a powerful tool to unravel intracrystalline deformation mechanisms (e.g. see Barber & Wenk 1976 for carbonate rocks). The disadvantage of calcite rocks in such studies is that it is difficult to prepare TEM-specimens with large domains of the appropriate thickness and that beam damage occurs relatively quickly, making it difficult to correlate TEM-observations with ordinary transmission optical microscopy (TOM) and rendering extensive tilt experiments impossible. Moreover, steady-state substructures become established after only a few per cent of strain (see, e.g. Durham *et al.* 1977 for olivine). It could, therefore, be argued that the observed substructures were established during late phases of deformation (e.g. uplift).

There exists now a wealth of data on experimental deformation of limestones (e.g. Heard 1963, Heard & Raleigh 1972, Rutter 1974, Schmid 1976, Schmid *et al.* 1977, 1980) and their microstructures and substructures including dislocation densities (Goetze & Kohlstedt 1977).

The aim of this paper is to see whether, or not, the substructures as observed using TEM in limestones from the Helvetic zone in eastern Switzerland, are the product of one particular phase of deformation as recognized by the field geologist, or whether later phases and regional uplift overprinted earlier substructures. In addition, by comparison with the results from experiments it was hoped to acquire some insight into the flow regimes (differential stresses) and deformation mechanisms responsible for the sub- and micro-structures encountered in the rocks. Finally, an attempt was made to bridge the gap between the different scales of TEM and TOM observations.

Geologic setting

The Helvetic zone in eastern Switzerland consists of two major units, the Helvetic nappes (Lower and Upper Glarus nappe complexes) above, and the Infrahelvetic complex below, separated by the Glarus overthrust (Fig. 1). Both the Helvetic nappes (e.g. Pfiffner 1981) and the Infrahelvetic complex (e.g. Pfiffner 1978) show an intricate internal structure characterized by folds and thrusts, accompanied by an axial planar thrust-parallel cleavage, and transverse tear faults (Calanda phase of Milnes & Pfiffner 1977, Pfiffner 1977, and phase 2 of Schmid 1975; see Table 1). The samples investigated were collected from the Infrahelvetic complex, where the Calanda-phase cleavage is more or less penetrative and from the footwall of the Glarus overthrust, where locally a second cleavage (Ruchi phase of Milnes & Pfiffner 1977, Pfiffner 1977, phase 3 of Schmid 1975) can be

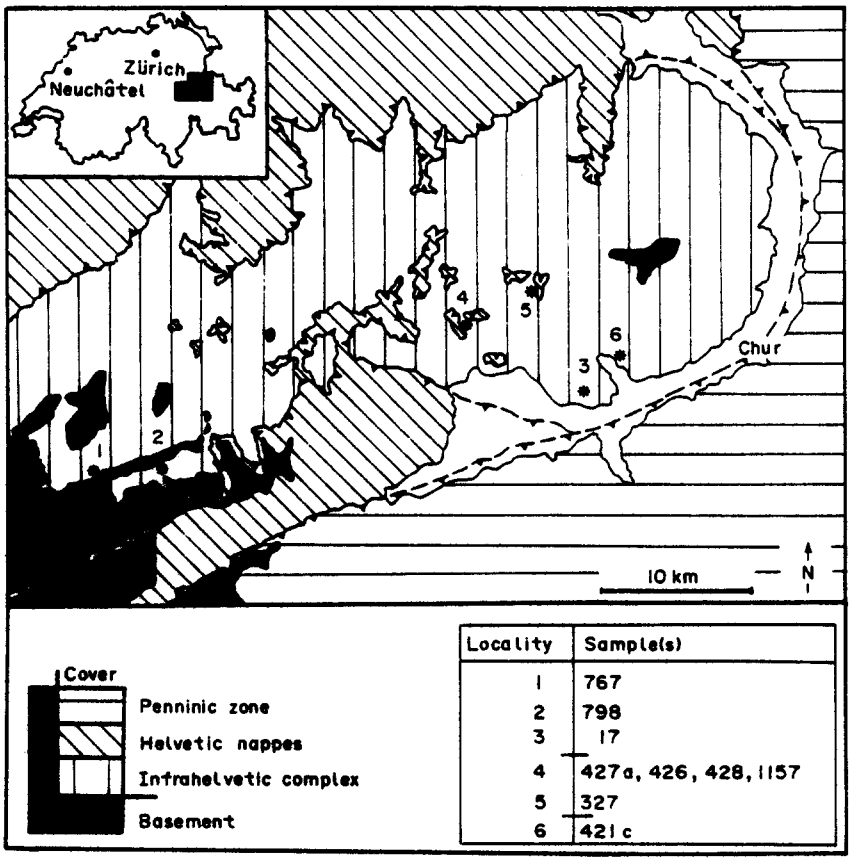

Fig. 1. Tectonic map showing sample locations and major structural units.

Table 1. Deformation phases and associated structures in the Helvetic zone of eastern Switzerland

	PHASE	SMALL SCALE STRUCTURES	LARGE SCALE STRUCTURES
PLIOCENE	phase not named	local cataclasis and heavy jointing	along reactivated transverse fault
MIOCENE	Ruchi phase	crenulation cleavage of patchy appearance	further northward transport of Helvetic nappes along Glarus overthrust with passive transport of earlier (Calanda phase) structures and inversion of metamorphic zonation
23 my	metamorphic event	growth of chloritoid	
M. - U. OLIGOCENE	Calanda phase	penetrative cleavage parallel to thrust faults and axial planar to folds	main phase of folding and thrusting in Infrahelvetic complex and Helvetic nappes -basement involvment -locally intricate successsion of folding and thrusting -transverse faults -development of Glarus overthrust -folding of Cavistrau phase thrusts
	Cavistrau phase	local cleavage parallel to thrust faults	large scale recumbent folding and emplacement of inverted limbs, thereby stripping off normal lying substratum (e.g. cover of Punteglias sub-massif, Fig. 2a)
	Pizol phase	none known	emplacement of exotic (flysch)strip sheets onto Helvetic zone, locally stripping off uppermost part of normal lying substratum
	youngest sediments affected: L. Oligocene		

The small-scale structures refer to the southern area shown in Fig. 1.

recognized. The cataclasite was collected from a reactivated transverse tear fault (Kunkelspass Querstörung, Pfiffner 1978), occurring within the Infrahelvetic complex.

The Infrahelvetic complex consists of a pre-Variscan crystalline basement and its mainly carbonate Mesozoic–Tertiary cover. Deformation within the basement shows progressively more ductile behaviour towards the more interior parts (basement wedges become more and more fold-like with the development of a penetrative schistosity). In the cover, folds include true buckle folds (Pfiffner 1980) and folds related to a staircase geometry of the thrust faults (ramps and flats). This staircase geometry was in most cases smoothed out by penetrative deformation (shear) in the footwalls of the faults, so that in many settings footwall ramps were transformed into synclines (see, e.g. the uppermost syncline below the Tschep nappe in Pfiffner (1978, fig. 5a), where a shear strain (γ) of over 40 is reached in the footwall).

The Glarus overthrust has a relatively smooth, arched surface (Milnes & Pfiffner 1980, Schmid 1975) and the displacement along its central portion is about 40 km. The deformation of the rocks along the fault is particularly concentrated in a 1–2 m thick calc–mylonite. This Lochseiten calc–mylonite is believed to be the product of smeared out Mesozoic limestones of the Infrahelvetic complex occurring in the immediate footwall of the thrust, acting as a lubricating layer at the base of the moving block. In the southern and central portion of the Glarus overthrust, the hangingwall rocks are mainly Permian conglomerates. For a further discussion of the Glarus overthrust, the reader is referred to Hsü (1969, mechanical model), Schmid (1975, mechanical model and field evidence), Pfiffner (1977) and Milnes & Pfiffner (1977, 1980; field evidence and tectonic evolution), Briegel & Goetze (1978, TEM study) and Schmid *et al.* (1981, textures).

The material studied

The limestones analysed can be divided into three groups, corresponding to three different deformation events.

(1) *The Infrahelvetic complex* (767, 17, 798). All samples are from the Middle Jurassic Blegi oolite and the finite strains (acquired during the pre-metamorphic Calanda phase) were analysed in an earlier paper (Pfiffner 1980, see also Table 2).

Sample 767 is a very slightly deformed specimen (the axial ratio of the finite strain ellipse in the plane analysed R_s = 1.27, corresponding to a stretching of e = 13%, Pfiffner 1977); it was collected from the 'strain shadow' of a large-scale boudin (sample locality Val Punteglias, co-ord. 716.230/183.100, see Fig. 2a) occurring near the Frisal thrust at the base of the Punteglias sub-massif basement wedge.

Sample 17 is a moderately deformed specimen (R_s = 3.1, Pfiffner 1980) from the normal limb of a large-scale fold (sample locality Denter Craps, co-ord. 748.000/188.900, see Fig. 2b), a block originally collected to study the homogeneity of strain at the scale of a hand specimen.

Sample 798 is a very highly deformed specimen (R_s > 12) from the footwall of the Cavistrau thrust; a thrust which carried in its hangingwall an already overturned sedimentary sequence, that during emplacement onto the Trun and Punteglias sub-massifs, stripped off most of the autochthonous cover from those sub-massifs (Fig. 2a). The block was collected from the extremely thinned-out remnants of the cover of the Punteglias sub-massif (sample locality Val Frisal, co-ord. 720.100/184.000).

The deformation in sample 17 can be attributed to the Calanda phase (Table 1), a phase of penetrative deformation characterized by the ductile behaviour of most rock types and the development of a regional cleavage (axial planar to folds and parallel to thrust faults). For sample 798 the deformation is due to the Cavistrau phase (Table 1), a precursor of the Calanda phase. Although the Cavistrau thrust was folded by the subsequent Calanda phase, the two phases cannot be separated on microstructural evidence. The minor deformation in sample 767 may be attributed to the Calanda and/or the Cavistrau phase.

The metamorphic event that occurred after the Calanda phase reached greenschist facies with temperatures of 350–400°C and pressures of 3–4 kbars for the rocks considered here (Frey 1978, Frey & Niggli 1971, Kisch 1974, Stalder & Touray 1970). Figure 3(a) shows a chloritoid rosette growing over the pre-existing Calanda phase cleavage.

(2) *The Glarus overthrust* (427a, 426, 428, 1157, 327). All the samples were collected at a location where limestones occur in the footwall of the Glarus overthrust. These limestones were mylonitized (Lochseiten calc–mylonite, see also Schmid 1975) and drawn out over a distance of at least 15 km along the thrust fault surface. Samples 427a, 426, 1157 represent a vertical section (sample locality Crap da Flem, co-ord. 739.450/193.550; see Fig. 2c) in a situation where the limestone (Schrattenkalk) underlying the Lochseiten calc–mylonite contains in its upper part highly deformed (mylonite-like) portions and the contact to the Lochseiten calc–mylonite proper is somewhat transitional (Fig. 2c, central portion). The same contact is very sharp in outcrop where sample 428 was collected (sample locality Crap da Flem, co-ord. 740.250/193.700; Fig. 2c).

The Glarus overthrust developed out of a major Calanda phase structure (Milnes & Pfiffner 1977), but movement along it also occurred during the following Ruchi phase, resulting in an inverse metamorphic zonation (Frey *et al.* 1974). During this Ruchi phase of transport a crenulation cleavage developed (Fig. 2c). As is characteristic of crenulation cleavages there must be a pre-existing anisotropy (bedding or early cleavage) before a crenulation can develop; this has resulted in the patchy appearance of the Ruchi phase crenulation cleavage, and in the limestones sampled one cannot observe any macroscopic effects of the Ruchi phase. Where

flysch occurs in the footwall of the Glarus overthrust, the lower boundary of the Lochseiten calc–mylonite is commonly folded into lobes (Fig. 2c, N portion) and the Ruchi phase crenulation cleavage is axial planar to the lobes. To study a possible overprinting of the submicrostructures of the earlier Calanda phase, this sample suite was collected from a structural setting where overprinting by this phase (the Ruchi phase) is probable, that is from immediately below the Lochseiten calc–mylonite.

Samples 1157 and 327 are Lochseiten calc–mylonites; a mylonite that has been investigated by Schmid *et al.* (1981) from a textural and microstructural point of view. Briegel & Goetze (1978) determined dislocation densities in this mylonite.

(3) *The cataclasite.* Sample 421c is an originally micritic Upper Jurassic (Quinten) limestone collected from the Kunkelspass transverse fault (sample locality Kunkelspass, 750.450/190.650; see Fig. 2b), a fault that was active during the Calanda phase (Pfiffner 1978), but which was later reactivated, resulting in local cataclasis. The bulk rock is heavily jointed and along bedding planes there are up to 10-cm thick cataclasite layers. The cataclasites contain rounded components of host rock swimming in an ultrafine, almost cohesionless rock-flour matrix; within the components the Calanda phase

Table 2. Sub- and microstructural parameters

SAMPLES	767	17	798	427a	426	425	1157	327	421c
SUBGRAIN SIZE in μm									
TOM -average	2.2	2.6	4.7	3.7	3.2	3.7			
-range	0.8 - 4	1 - 4	3 - 8	2 - 5	1 - 5	1.5 - 5			
TEM -mean	1.9	1.9	2.7	1.1	3.3	2.9			2.6
-stand. deviation interval	0.2-3.6	0.7-3.6	0.7-3.7	0.4-1.8	1.9-4.5	2.0-3.7			0.4-4.8
-spacing of walls and networks			1.2-2.9	0.9-1.8		2.5			
TEM									
number of large grains observed N	13	17	10	11	28	25			25
number of micro-twins observed T	2	2	3	1	7	13			14
twin frequency T/N	0.15	0.12	0.33	0.10	0.46	0.28			0.56
average free dislocation density in cm^{-2}	2.7×10^9	3.0×10^9	2.7×10^9	2.2×10^9	3.1×10^9	3.3×10^9			
unique TEM-features	D	D	D						G
TOM									
subgrain size in μm	2.2	2.6	4.7	3.7	3.7	3.2	3.5	9.0	
mean size of grains (d=1/g) in μm	3.35	4.00	9.83	6.43	8.60	6.17	4.50	11.51	
max. size of large dyn. recr. grains, μm	15	30	40	25	20	20		50	
grain shape aspect ratio r	1.01	1.25	1.48	1.59	1.23	1.24	1.26	1.28	
degree of shape preferred orient. Ω	0.005	0.136	0.232	0.272	0.129	0.132	0.143	0.150	
finite strain axial ratio R_s	1.27	3.1	>12						
DIFF. STRESS σ_D in bars estimated with:									
disl. densities (α=1)	840	850	840	750	870	900	730-1100*		
subgrain size (Schmid et al. 1980)	2000	1900	1000	1200	1200	1300	1250	510	
subgrain size (Twiss 1977)	1400	1300	700	900	900	950	920	350	
mean size of grains (Twiss 1977)	4000	3500	1900	2300	2000	2500	3200	1900	
max. size of large dyn. recr. grains (Twiss 1977)	1400	920	750	1000	1300	1300		620	
TECTONIC SETTING	Infrahelvetic complex			footwall Glarus overthrust			mylonite		cataclasite

D, dislocation-free subgrains; G, very long, straight glide-dislocations and ring patterns in diffraction: *, after data from Briegel & Goetze (1978).

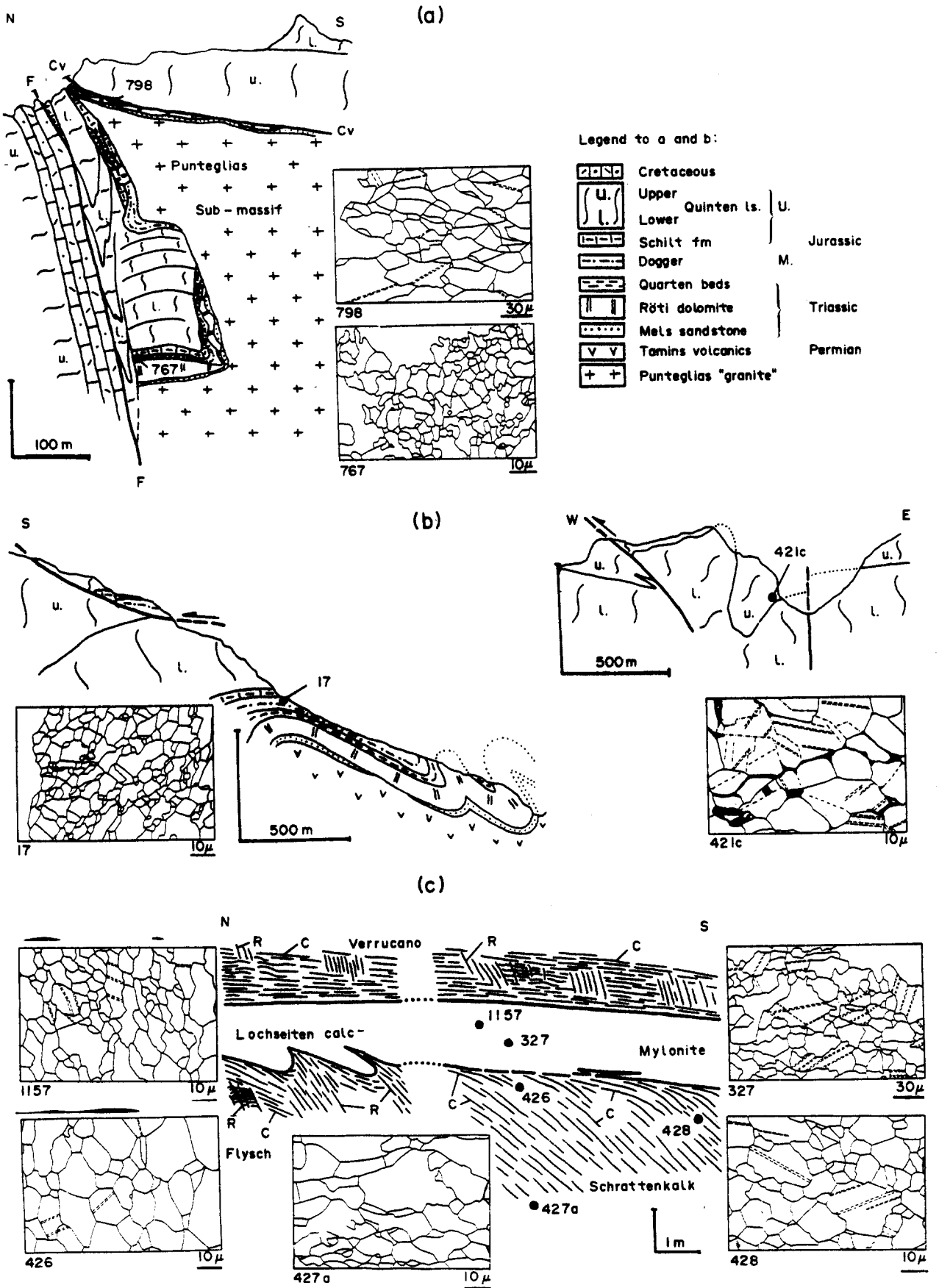

Fig. 2. Profiles showing structural settings of samples. Insets are line diagrams of microstructures. (a) Punteglias sub-massif is thrust along the Frisal thrust fault (F) onto the sedimentary cover. The sequence in the hangingwall of the Cavistrau thrust faul (Cv) is overturned. (b) Profile through fold structure of sample 17 is nearly perpendicular to the regional strike, profile through the Kunkelspass transverse fault (sample 421c) is nearly parallel to regional strike. (c) Synoptic profile for the Glarus overthrust, marked by the Lochseiten calc–mylonite. Note lobes formed by lower limit of the mylonite where it is underlain by flysch and the angular relations between the Calanda phase (C) and Ruchi phase (R) cleavages.

cleavage (shape preferred orientation of the calcite crystallites) is preserved (Fig. 3b).

Methods used

Prior to ion thinning the thin sections of about 20 μm thickness were prepared, polished on both sides using diamond paste (> 2μm). Ion thinning was performed on a Technics Inc. ion milling machine using 4–5 kV and a rotating stage inclination of 14°. The samples were then coated with Carbon and analysed on a Philips EM400 (max 120 kV).

The TEM samples were also observed on an ordinary transmission optical microscope (TOM) as substantial portions of the ion-thinned sections were less than 5 μm thick, allowing subgrains to be seen without overlap effects. To determine grain and subgrain sizes a series of photographs was taken under crossed polarizers, rotating the specimen in 30° intervals about the microscope axis. This procedure was necessary to make all the subgrain boundaries visible; working on single photographs would have resulted in substantial overestimates. It was found that after the superposition of three such photographs practically all subgrain boundaries were recorded.

The grain sizes were determined by the intercept method (Snyder & Graff 1938) which consists of counting the number of (low and high angle) boundaries intersected along linear traverses at random points (see also Nicolas & Poirier 1976, p. 338) on line diagrams (shown in Fig. 2) which were prepared from superimposed photographs (method explained above). The subgrain sizes were determined by selecting individual subgrains under the microscope and comparing these with the line diagrams.

The determination of the dislocation density was achieved using the random-line intercept method described by Ham (1961); the thicknesses of the foils were measured by tilt experiments on planar interfaces and dislocations viewed head-on.

RESULTS

The results are summarized in Figs. 2 (insets), 3 and 4 and in Table 2.

The Infrahelvetic complex

(1) *Transmission optical microscopy*. The microstructures are displayed in Figs. 3(c) and 2 (insets in a and b).

Three types of grains can be recognized: large (15–40 μm) and intermediate (8–30 μm) size grains and subgrains (2–5 μm). The large and intermediate size grains show a shape-preferred orientation, but their aspect ratio is smaller than the corresponding ratio of the strain ellipse. The subgrains are more equant and have straight boundaries. The optically determined subgrain size seems to be somewhat larger than the one obtained from the TEM study. This is because the TEM value is a mean value of all the grains observed (i.e. including those which represent marginal cuts), while for the TOM-value, subgrains were selected individually and the value in Table 2 represents an average value for cuts nearly through their centres. The grain boundaries of the large and intermediate sized grains are serrate in the case of the slightly deformed rocks (767) whereas they are remarkably straight in the moderately and highly deformed ones (17 and 798) commonly forming 120° angles at triple points.

The average grain size was obtained by the intercept method (Snyder & Graff 1938), but using the formulas given by Nicolas & Poirier (1976, p. 338) with $1/g$ being the average diameter. It represents an average of all the three grain types mentioned above. The aspect ratio and degree of preferred orientation were calculated on the basis of the same data. The listed aspect ratios are $1/r_{x/z}$ in the terminology of Nicolas & Poirier (1976, p. 338) and Ω assumes the values 0 and 1 for completely random and completely oriented structures, respectively (cf. Rack & Newman, in Cahn 1970, p. 760).

As is evident from Table 2, the subgrain size, the average grain size, the maximum size of large grains, the aspect ratio and the degree of preferred orientation is seen to increase with increasing amount of finite strain.

(2) *Transmission electron microscopy*. There are a number of substructure features which can be observed in all the samples from the Infrahelvetic complex, as well as in all the samples from the Glarus overthrust and partly even in the cataclasite. They include:

(a) areas of low dislocation density (approaching zero in some instances) within large and intermediate size grains;

(b) low-angle tilt and twist boundaries within large and intermediate size grains;

(c) dislocations forming loops, dipoles, pinching-off dipoles and cusps;

(d) dislocation interaction and three-dimensional tangles;

(e) jogged dislocations;

(f) arrays of dislocations with straight, parallel segments and

(g) polygonized subgrains.

Note that this list includes features indicative for both hot and cold work conditions.

A substructure type that could not be observed is the cell structure with bands of high dislocation densities separating domains of relatively lower dislocation density typical for cold-working in metals.

In addition to the common features of the substructure (a)–(g), the following characteristics could also be observed.

(h) The densities of the free dislocations in intermediate and large-size grains (grains with a diameter exceeding 6 μm) is the same for all samples in this suite although each suffered variable amounts of strain.

(i) Tilt experiments indicated that dislocation-free subgrains (Fig. 4a) do occur. Some small grains which contain dislocations possibly represent marginal cuts of intermediate or large-size grains.

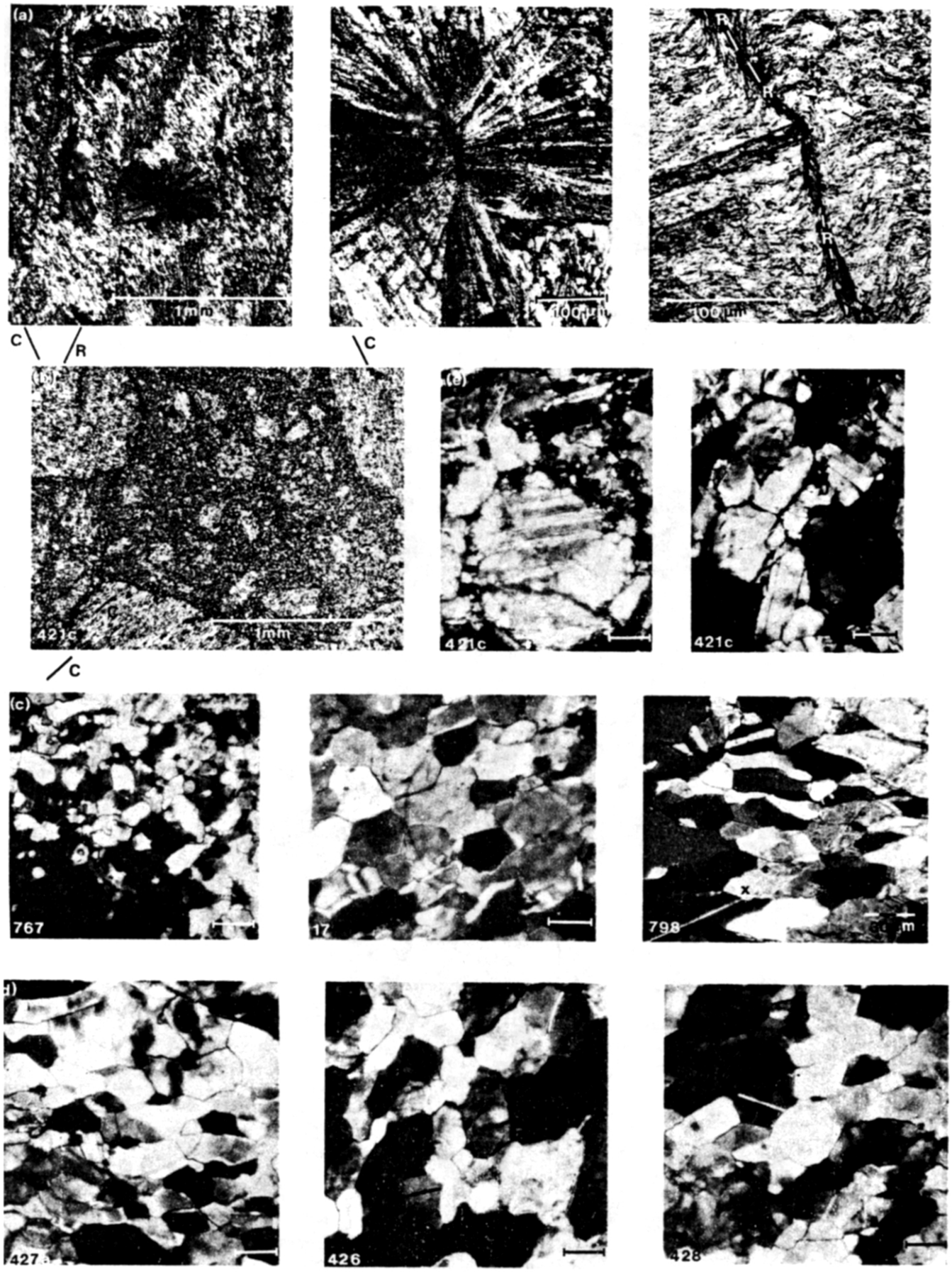

Fig. 3. TOM-micrographs. Where not otherwise stated, the bar-scale is 10 µm. Crossed polarizers in (b)–(e) inclusive. (a) Relation between growth of chloritoid and Calanda phase (C) and Ruchi phase (R) cleavages. Shales from Quartenschiefer formation. (b) Cataclasite: rounded components (pale) containing Calanda phase cleavage (C) set in very fine-grained matrix (dark). (c) Infrahelvetic complex. Note development of shape-preferred orientation from 767 to 798 and deflected microtwin at x in 798. (d) Footwall of Glarus overthrust. Note weaker shape preferred orientation, straight grain boundaries and microtwins closer to the mylonite (426 and 428). (e) Cataclasite: very small grains near broadened, initially straight grain boundaries and twins.

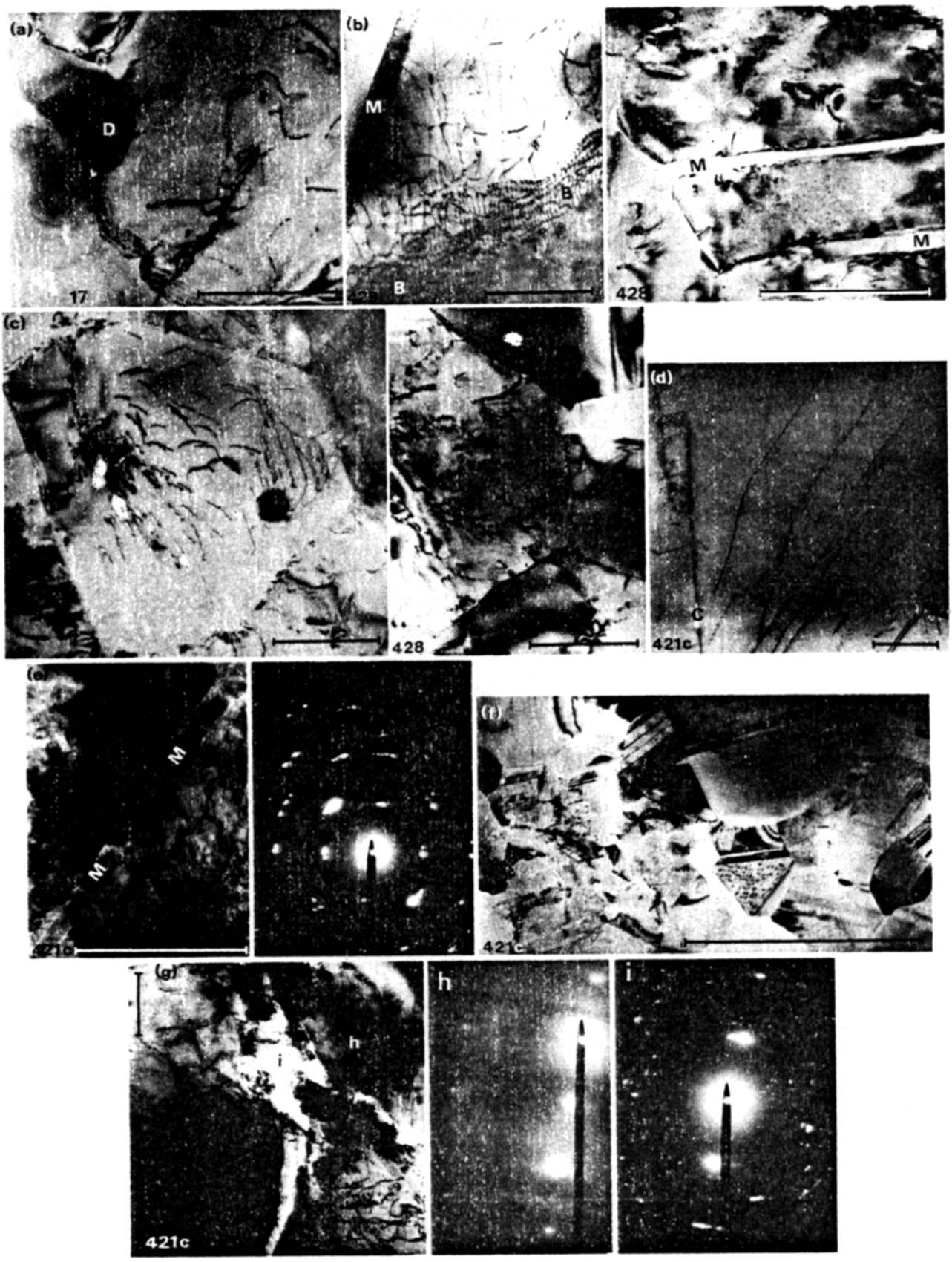

Fig. 4. TEM-micrographs. Bar-scale is 1 μm. (a) Dislocation-free sub-grain (D). (b) Straight microtwins (M) and low-angle twist boundary (B). (c) Straight grain boundaries causing polygonal substructure. (d) Very long straight glide-dislocations and cleavage (C) in large grain from within component. (e) Shattered large grain with hardly recognizable microtwin (M) and incipient ring pattern in diffraction. (f) Very small and heavily twinned grains from matrix. (g) *In situ* cataclasis. BF-image with location of diffractograms. (h) Regular pattern in healthy portion. (i) Incipient ring pattern due to cataclasis.

(j) With the exception of 798 (collected from the footwall of a thrust fault) twin lamellae were rarely observed.

The Glarus overthrust

(1) *Transmission optical microscopy*. The microstructures are displayed in Figs. 3(d) and 2 (insets in c). As in the Infrahelvetic complex, three types of grains can be distinguished: large (20–25 and 50 μm) and intermediate (10–15 and 20–30 μm) size grains and subgrains (3–4 and 9 μm). The large and intermediate size grains again show a shape-preferred orientation. The grain boundaries are straight and meet at 120° angles in triple points. The equi-axial subgrains have a constant size lying between the moderately and highly deformed samples from the Infrahelvetic complex. The resulting polygonal substructure is indistinguishable from the one observed in those samples. With the exception of the size of the large grains, all the parameters lie somewhere between the moderately and highly deformed rocks of the Infrahelvetic complex.

(2) *Transmission electron microscopy*. Besides the common substructure features (a)–(g) listed above the following features are characteristic.

(h) The free dislocation density in large and intermediate-size grains (6 μm) is again more or less constant and also identical to the one found in the Infrahelvetic complex. The relatively low density in 427a does not seem to be of significance if one takes the relatively large scatter of the data of Briegel & Goetze (1978) into account.

(i) As opposed to the Infrahelvetic complex not a single dislocation-free subgrain was found in this suite.

(j) The samples contain more microtwins, particularly the ones immediately underlying the thrust fault (426 and 428); this is especially true for the Lochseiten calc–mylonite. However, even where there is 'heavy' twinning, it represents a very small amount of strain. Remarkable again is the absence of any cell structure as noted in the Infrahelvetic complex.

The cataclasite

(1) *Transmission optical microscopy*. The components show a microstructure (Figs. 3e and 2b, inset) in part comparable to that described for the rocks from the Infrahelvetic complex and Glarus overthrust. The difference is that the grain boundaries are seen to be broader. Thus, one can in some instances observe a relict microstructure with straight grain boundaries meeting at triple points forming angles of 120°, but where the grain boundaries are very broad they become somewhat diffuse and nothing can be inferred about their initial nature (black in Fig. 2b). The large and intermediate size grains contain microtwins.

The matrix cannot be resolved optically.

(2) *Transmission electron microscopy*. The following features are typical for the components (cf. Figs. 4d, e & g):

(a) Absence of dislocation-free subgrains.

(b) Quite common occurrence of microtwins in large and intermediate size grains.

(c) Existence of very long straight glide-dislocations in large grains, not observed in the other rock suites (Fig. 4d).

(d) Appearance of incipient cleavage within the large-size grains (sets of parallel planar features which do not compare with twin, grain or subgrain boundaries; Fig. 4d).

(e) Occurrence of ring patterns within large grains (Fig. 4g). The microstructure of the latter in these cases is diffuse (see, e.g. the hardly recognizable microtwin in Fig. 4e). It is interpreted that the areas where ring patterns occur correspond to the broadened diffuse-looking grain boundaries seen under the optical microscope.

In the matrix the characteristic features include: (a) the occurrence of very small grains (0.1 to 0.3 μm in diameter) and (b) heavy twinning of these very small grains (Fig. 4f).

In some of these grains no dislocations could be found; this is compatible with the observation that the free dislocations within large-size grains are somewhat inhomogeneously distributed such that areas comparable in size to these very small grains exist which are 'dislocation-free'. Thus if the very small grains had formed by breaking up of the larger grains, dislocation free individuals have to be expected. Noteworthy is the absence of a cell structure typical for cold-working in metals.

DISCUSSION AND CONCLUSIONS

Applicability of transmission electron microscopy

As it takes only a relatively small amount of strain to form a substructure and set a dislocation density, the possible effects of overprinting by later deformational events have always to be kept in mind. The latest event common to all the samples was uplift (amounting to 12–15 km for the Infrahelvetic suite). Therefore, could the observed dislocation densities, which are surprisingly constant in all of the investigated samples, be due to uplift? The fact that dislocation-free subgrains occur, and only occur in the Infrahelvetic complex, is evidence against this hypothesis. It seems rather that the strains due to uplift are not penetrative, but rather may be concentrated in uplift-accommodating faults. This does not mean that the blocks lying between the faults and escaping being strained did not support differential stresses: it can be shown (Pfiffner & Ramsay 1982) that if the strain rate was slower than 10^{-15} s^{-1} the strains picked up within the available time (20 Ma) will be too small ($\ll 1\%$) to reset the dislocation densities. If recent uplift rates are taken (Schaer & Jeanrichard 1974 for the Gotthard traverse; Gubler 1976, from which a section

through the sample localities can be established) a strain rate of $\dot{\varepsilon} = 3 \times 10^{-16}$ s^{-1} can be calculated, and during the last 20 Ma uplift-rates seem to have been relatively constant (Schaer 1979). The strain rates mentioned above were calculated by treating the actual uplift as a vertical broad shear zone, a model which closely fits the recent uplift data; thus, deformation is assumed to have occurred homogeneously throughout the uplifting block. This is not very likely to occur, but is necessary to explain constant dislocation densities throughout the area investigated. Faults which could possibly be related to recent uplift do occur in the general area investigated and were carefully avoided.

Topographic relief, which causes differential stresses, cannot explain the observed dislocation densities either: the Infrahelvetic suite (containing dislocation-free subgrains) was sampled on Alpine valley slopes, and the samples from the Glarus overthrust were collected on flat mountain tops.

As the substructures record only the last few per cent of the strain, the deformation mechanism which led to the formation of dislocation-free subgrains in the Infrahelvetic complex seems to have been active to the last increments of strain that these rocks experienced in their deformational history; a deformational history characterized by rising temperatures (pre-metamorphic Cavistrau and Calanda phases). In particular, the substructure shows that no shift to some other mechanisms (e.g. cold-working or twinning) occurred, a point which only a TEM-study could reveal. On the other hand, in the footwall of the Glarus overthrust, where effects of the post-metamorphic Ruchi phase are most likely to have occurred, no such dislocation-free subgrains could be found. A careful TEM-study, therefore, allows us to distinguish between the pre- and post-metamorphic deformation phases recognized by the field geologist. The nature of the debris observed within the large and intermediate sized grains is the same throughout all the samples (except the cataclasite) and, hence, their analysis does not seem to be a powerful tool to determine deformation mechanisms in naturally-deformed rocks.

The twinning observed in samples from footwalls of thrust faults (798, 428, 426) is a late event (discussed below) and could be due to changes towards higher stresses, possibly accompanied by a drop in temperature towards the close of the deformation. As the dislocation densities in those same samples are not significantly different, the strains due to the deformational event producing the twins (e.g. a late strain pulse along the thrust faults) were too small (less than 1%) to reset the densities.

Deformation mechanisms

As all the rocks analysed recrystallized at some stage of their deformation and a metamorphic event occurred either before or after these deformation phases (Table 1), the role of recrystallization needs to be carefully assessed (for a discussion of recrystallization see Cahn 1970, Cotterill & Mould 1976).

(1) *The Infrahelvetic complex.* Remembering that a metamorphic event occurred after the microstructure was established (Fig. 3a and Table 1), the effects of static recrystallization must be carefully considered. Static recrystallization is characterized by equant grains, straight grain boundaries and low dislocation density, while dynamic (syntectonic) recrystallized in dislocation creep leads to flattened grains, ragged grain boundaries and a polygonized substructure (Nicolas & Poirier 1976). In the rocks from the Infrahelvetic complex, the large and intermediate size grains appear to have flattened while suffering strain (the aspect ratio increases with increasing amount of strain, see Table 2), and at the same time they show a polygonized substructure with dislocation free subgrains (Figs. 4a & c). Thus, dynamic recrystallization seems plausible. On the other hand, the high-angle grain boundaries are remarkably straight, and not ragged; therefore, some grain boundary migration must have occurred. This fact is also indicated by the pinning of (more mobile) high-angle boundaries by (more sessile) low-angle boundaries, which is frequently observed (Fig. 3c).

We might also enquire if such a grain boundary migration under conditions of static recrystallization also explains the aspect ratio of the crystallites being smaller than the axial ratio of the strain ellipse? As sweeping high-angle grain boundaries are likely to wipe out very efficiently any shape-prefered orientation, this process does not seem probable. Moreover, the existence of the polygonized substructure and the associated dislocation densities argue against a thorough overprint by static recrystallization. The low aspect ratio of the crystallites could more easily be explained by grain boundary sliding, a process in which bulk-rock strain is accommodated by grains sliding past each other. In the extreme case, that of superplastic flow, most of the bulk strain is accommodated by grain boundary sliding and the microstructure is characterized by equant grains and the absence of a polygonized substructure.

The constant free dislocation density in the large and intermediate size grains is in agreement with that found in experimentally deformed fine-grained limestones in the dislocation power-law creep regime (Schmid *et al.* 1977, regime 2), for which a bulk diffusional process as the rate-controlling step for glide was suggested. However, the straight grain boundaries and the fluctuation in free dislocation density resulting if subgrains are also considered compare with the superplastic flow regime (regime 3 of Schmid *et al.* 1977). It is, therefore, concluded that the rocks in the Infrahelvetic complex deformed in a region between the fields of power-law creep and superplastic flow, that is by dislocation creep accompanied by substantial grain boundary sliding, and that the stress exponent, n, in the constitutive equation was somewhere between 2 and 5.

The twinning observed in 798 (collected in the footwall of the Cavistrau thrust) represents a very small amount of strain because only a few grains show very

thin twin lamellae (microtwins). It seems to have occurred after the development of the microstructures discussed above because the lamellae run entirely through individual grains (offsetting their boundaries) and, notably, are never lensoid as is characteristic of rocks deforming mainly by twinning under metamorphic temperatures (Schmid *et al.* 1980). In any case, this twinning event seems to represent a late strain pulse and it did not reset the dislocation densities. The rarely observed microtwins in samples 767 and 17, representing an even smaller strain, could be due to regional uplift.

A different type of twins exist in fossil fragments: they may be curved, lensoid and show serrate boundaries which indicate twin boundary migration. Hence, these twins must have formed early in the deformational history (Cavistrau and early Calanda phases).

(2) *The Glarus overthrust.* The microstructures in the rocks collected in the footwall of the Glarus overthrust are essentially the same as the ones just discussed in the Infrahelvetic complex collected at deeper levels (around 1 km below the Glarus overthrust). Thus, the large and intermediate size grains show a shape-preferred orientation and a polygonized substructure with straight grain boundaries. The aspect ratio, however, decreases as one approaches the thrust fault, although higher (shear) strains would be expected. This points to grain boundary sliding becoming the dominant deformation mechanism and hence a shift towards superplastic flow (regime 3 of Schmid *et al.* 1977, 1980). On the other hand, no dislocation-free subgrains were found in these rocks. Thus, these samples seem to have deformed between the fields of power law creep and superplastic flow similarly to the ones in the Infrahelvetic complex. However, grain boundary sliding was more important and a shift to power law creep (higher stresses) took place at later stages (indicated by the homogenization of the free dislocation density). This is also the only effect that can be specifically attributed to the Ruchi phase.

The twinning which becomes more obvious as one approaches the Glarus overthrust is again of the type of straight thin lamellae usually running through entire individual grains, offsetting their grain boundaries, that is a very small amount of strain imposed after the above mentioned micro- and substructures had already been established. Nevertheless it points to a shift to still higher stresses typical for rocks deforming mainly by mechanical twinning (Schmid *et al.* 1977, regime 1). Moreover, this twinning affected only the large and intermediate size grains ($d > 5\mu m$) and never subgrains. It does not seem to be important enough to be correlated with the Ruchi phase nappe transport which created the inverse metamorphic zonation.

The situation is different in the Lochseiten calc–mylonite which is found along the Glarus overthrust. When looking at this mylonite from the point of view of its structural position, two areas have to be distinguished: a northern section corresponding to a more external, shallower portion of the thrust fault at the time of its activity (north of the present day antiformal arch) and a southern section of more internal, deeper origin, from which the investigated samples were collected. In the northern section, the Lochseiten calc–mylonite shows neither a macroscopic stretching lineation nor a crystallographic preferred orientation, and the dominant deformation mechanism as indicated by the present-day micro-structures and textures, is grain boundary sliding in superplastic flow (Schmid *et al.* 1981, sample 6 and possibly the matrix of sample 63). In the southern section, a macroscopic stretching lineation parallel to the probable movement direction of the nappe pile (Pfiffner 1981) may be observed in some portions of the mylonite. Moreover, the microstructure shows a shape-preferred orientation in these cases (sample 1157; Fig. 2c); this shape-preferred orientation is confirmed in sample 327 collected from a structurally similar situation 5 km farther east–north east along strike (locality Ringelspitz, co-ord. 745.000/195.000). Sample 115 of Schmid *et al.* (1981) was collected at the same general location as 327 and it shows only a weak crystallographic preferred orientation. This led Schmidt *et al.* (1981) to the conclusion that the rock deformed by superplastic flow. Thus, although a lot of strain is concentrated in the Lochseiten calc–mylonite, in the southern section superplastic flow (with typically equant grains) occurred only in portions of the mylonite, while the rest deformed similarly to the rocks in the footwall of the Lochseiten calc-mylonite, that is somewhere between the fields of power-law dislocation creep and superplastic flow (flattened grains).

The above rocks, forming the footwall of the thrust belong to the Lower Cretaceous Schrattenkalk formation, that is they were initially limestones containing large intraclasts in either a micritic or a sparitic matrix (Briegel 1972). As the initial grain-size distribution is not clear, an interpretation of their evolution is rendered difficult. This fact is also evident from the variable types of mylonites that can be distinguished: In particular, 327 shows a relatively homogeneous grain size, whereas 1157 contains large intraclasts that are heavily twinned and recrystallized, and an intermediate size (9 μm) and small size (4.5 μm) matrix forming bands and flowing around the drawn-out intraclasts. A 'homogenization' of the grain size (grain growth within the micritic matrix, polygonization of the intraclasts) was found in similar limestones (from the Oehrlikalk formation) collected in the footwall of a Calanda phase thrust within the Infrahelvetic complex close to the fault contact (Pfiffner 1977) and possibly it means that the rocks tried to achieve an 'equilibrium grain-size'.

The late twinning event recognized in the footwall is also to be observed within the Lochseiten calc–mylonite, but, unlike in the footwall, twinning also occurred in the smaller-sized grains. This is confirmed by the TEM study of Briegel & Goetze (1978, fig. 2). At the same time, the microstructures that developed prior to the twinning event are not too different if one compares the footwall and the Lochseiten calc–mylonite in the southern section. Thus, the differential stresses associated with the twinning event were higher in the

mylonite than in the footwall: had they been equal or lower, twinning would have been restricted to the large-sized grains or a shift in deformation mechanism from power-law dislocation creep to mechanical twinning would not have occurred.

In conclusion, a combined TEM/TOM/field study reveals that the Glarus overthrust is a ductile fault where an increasing amount of shear strain close to the mylonite was accommodated by grain boundary sliding, which itself became relatively more important (shift to superplastic flow). Viewed in time, the deformation mechanisms then shifted to power-law creep and twinning, that is to higher differential stresses, together with a probable drop in temperature due to erosion.

(3) *The cataclasite*. The deformation mechanisms in the cataclasites subsequent to the hot-working during the Calanda phase were of a brittle nature. In the components it included the modification of the nature of high-angle grain boundaries as seen by their broadening. Besides microtwinning the grains are seen to break up (cleavage) and to decompose into very small grain fragments (0.1–0.3 μm) giving rise to areas showing ring diffraction patterns (Figs. 4e & i). Strain within the ultrafine-grained matrix must have been substantial as it has to allow for significant rotations of the components and for their rounded shape (Fig. 3b). Deformation mechanisms in the matrix include heavy mechanical twinning of the grain fragments with a diameter as small as 0.1–0.3 μm, possibly indicating high differential stresses. A geologic interpretation is not easy because the dating of the cataclasis is as yet not possible (other than that it occurs along a Calanda phase reactivated fault). Nevertheless it is interesting to note that the incipient brittle deformation occurs mainly along the grain boundaries.

Palaeostress estimates

One aim of this work was to see whether it is possible to get an estimate of the differential stresses which brought about the microstructural changes. Palaeostress piezometers that have been proposed include dislocation density, the size of subgrains and the size of dynamically recrystallized grains.

It is found that for many materials the dislocation densities increase with increasing stress according to the following relation

$$\sigma_D = \sigma_1 - \sigma_3 = \alpha \mu \mathbf{b} \varrho^{1/2}. \quad (1)$$

In this relation, α is a constant near 1 for many materials in both hot- and cold-working (Goetze & Kohlstedt 1977), μ is the shear modulus, **b** is the Burgers vector and ϱ is the dislocation density. Experimental calibrations have been carried out in Yule marble (Goetze & Kohlstedt 1977), Solenhofen limestone (Schmid *et al.* 1977, Briegel & Goetze 1978) and Carrara marble (Schmid *et al.* 1980). These results are compiled in Fig. 5(a).

In addition, Twiss (1977) concluded, on the basis of a theoretical study, that both the size of subgrains and the size of dynamically recrystallized grains should decrease with increasing differential stress. Schmid *et al.* (1980) calibrated the relationship for the size of equant new grains in Carrara marble. All these curves are given in Fig. 5(b).

The results of stress determinations made from rocks used for this study obtained by using these various curves are listed in Table 2 and are now discussed in some detail.

(1) *The Infrahelvetic complex*. The average free dislocation density (3×10^9 cm^{-2}) measured in the large and intermediate sized grains in these originally micritic rocks compares to the one obtained in experimentally deformed micritic (Solenhofen) limestone within any of the three flow regimes reported by Schmid *et al.* (1977), whence σ_D would lie between 200 bars and 1 kbar. From microstructural arguments mechanical twinning, as occurs in regime 1 in the case of Solenhofen limestone,

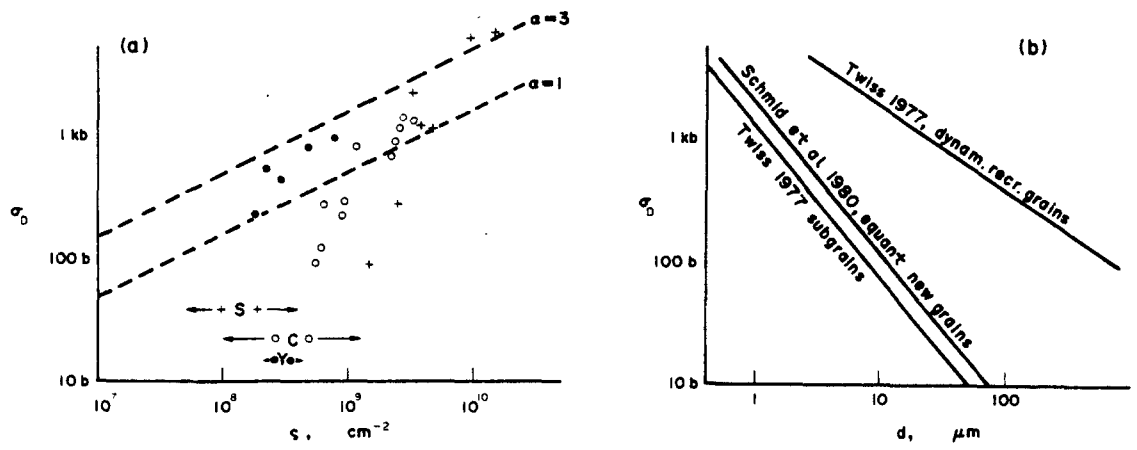

Fig. 5. Experimentally obtained relation between differential stress, σ_D, and dislocation density, ϱ, in (a) and sizes d of various grain types in (b). The lines for $\alpha = 1$ and 3 in (a) are given for comparison only. Arrows show range of dislocation densities of the starting material. Y, Yule marble; C, Carrara marble; S, Solenhofen limestone.

can be excluded. However, Schmid *et al.* (1977) pointed out that care has to be taken when using the dislocation density as a piezometer, since they believe that their densities were partly established during cooling and unjacketing and are, thus, not really representative for the differential stresses at steady state. The values of 840–850 bars given in Table 2 correspond to $\alpha = 1$ in equation (1).

If the size of the equant subgrains is taken as a piezometer, higher values for differential stress are obtained (with the exception of sample 798). This discrepancy is not understood. Because cooling and unjacketing of the experimentally deformed samples would increase the dislocation density, this source of error does not offer an explanation.

The mean size of the grains yields still higher values. As for the determination of this parameter, all types of grains, subgrains, intermediate and large sized grains were used, the result probably means that the parameter chosen (average of all sizes) is not appropriate.

If the maximum size of the dynamically recrystallized grains is taken, a surprisingly good agreement is obtained with the theoretically derived curve of Twiss (1977) for subgrain size. The corresponding differential stresses are consistently lower than those obtained if the subgrain size curve of Schmid *et al.* (1980, fig 20) is taken. It has to be noted also that their TOM-values are systematically higher than their TEM-values, a discrepancy not found in this study. It will be noted that the stress estimates based on the size of subgrains and the maximum size of the dynamically recrystallized grains correspond more or less with those indicated by the dislocation density.

(2) *The Glarus overthrust.* In the footwall the dislocation densities are more homogeneous, but otherwise much the same as those in the Infrahelvetic complex. It is not clear what type of matrix the material originally had (micritic or sparitic) and, hence, one does not know which experimental material should be used for extrapolation. Taking marble, the interval is 0.6–1.2 kbars, whereas for micritic Solenhofen limestone it is 0.2–1.2kbars (Fig. 5a). The values of 750–900 bars given in Table 2 again correspond to using $\alpha = 1$ in equation (1).

As for the grain sizes in these rocks, good agreement between the estimates from the maximum size of the large (dynamically recrystallized) grains and subgrain size is obtained for 427a by using the Twiss curves (a differential stress of ~1 kbar seems to be indicated). Similarly to what was found in the Infrahelvetic complex, the mean grain size yields an unrealistically high differential stress. For 426 and 428 (both collected immediately below the Lochseiten calc–mylonite), the above mentioned agreement breaks down: the maximum size of the dynamically recrystallized grains gives higher stresses (1.3 kbars) than the subgrain size, but the latter gives the same stresses as dislocation densities (around 900 bars). These changes in 'agreement' and 'discrepancy' may well reflect the change in deformation mechanism towards grain boundary sliding (discussed earlier), and possibly the onset of grain growth inhibition (resulting in high stress estimates from the large dynamically recrystallized grains).

The situation in the Lochseiten calc–mylonite is even more complex due to the different types of mylonite coexisting, having variable grain sizes and grain size distributions.

Thus, as has been pointed out by Schmid (1981 unpublished thesis), different deformation mechanisms seem to go on in different portions of the mylonite and it is, therefore, extremely difficult to give an estimate for the active differential stresses. Briegel & Goetze (1978) estimated the differential stresses to be of the order of 1–2.8 kbars based on dislocation densities, but argued that this could represent the differential stress at the latest stage. If α in equation (1) is taken as one, their dislocation densities would correspond to differential stresses of 0.73–1.1 kbars. The subgrain sizes cannot readily be used, because, for example, the calibration curve of Schmid *et al.* (1980) is valid only for subgrains that formed by progressive rotation (in particular not by nucleation); the subgrain size of the Lochseiten calc–mylonite sample 63 (Foostock) reported by Schmid *et al.* (1981) is less than a few μm, and this sample occurs in a situation comparable to the one of Briegel & Goetze (1978). In this general area, situated 10 km north of the outcrop studied in this work, no macroscopically visible stretching lineation exists in the mylonite and the rocks deformed mainly by grain boundary sliding as discussed earlier.

In the southern section, including the outcrops investigated, the Lochseiten calc–mylonite does show a stretching lineation and the dynamically recrystallized grains are flattened. Thus, the deformation mechanisms seem to be more comparable to those in the footwall described earlier. If now the same calibration curves are used (Fig. 5b), differential stresses turn out to be of the order of 350–600 bars (327) and 0.9–1.25 kbars (1157, fine-grained matrix), compared to ~1 kbar for the footwall rocks.

Acknowledgements—The TEM-work was supported by grant number 0.330.066.01/0 from the ETH-Zurich, and by the Schweizerischer Nationalfonds project number 2.859.0.77. The work was completed at the University of Neuchâtel. The author wishes to thank the thin-section laboratory of the Earth Science Department and the TEM-laboratory of the Institute of Metallurgical Research in Zurich for technical assistance, Ken Hsü and John Ramsay for providing the funds, and Geoff Milnes for correcting his English. He profited from discussion with W. Form, Rick Groshong, Stefan Schmid, Ueli Briegel and J. P. Schaer. This paper is a shortened and modified version of the author's habilitation thesis at the University of Neuchâtel.

REFERENCES

Barber, D. J. & Wenk, H.-R. 1976. Defects in deformed calcite and carbonate rocks. In: *Electron Microscopy in Mineralogy* (edited by Wenk, H.-R.) Springer, Berlin, 428–442.

Briegel, U. 1972. Geologie der östlichen Alviergruppe unter besonderer Berücksichtigung der Drusberg- und Schrattenkalkformation. *Eclog. geol. Helv.* **65**, 425–483.

Briegel, U. & Goetze, C. 1978. Estimates of differential stress recorded in the dislocation structure of Lochseiten limestone (Switzerland). *Tectonophysics* **48**, 61–76.

Cahn, R. W. 1970. Recovery and recrystallization. In: *Physical Metallurgy* (edited by Cahn, R. W.). Elsevier/North-Holland, Amsterdam, 1129–1197.

Cotterill, P. & Mould, P. R. 1976. *Recrystallization and Grain Growth in Metals*. Surrey University Press, Yeovil, U.K.

Durham, W. B., Goetze, C. & Blake, B. 1977. Plastic flow of oriented single crystals of olivine—2. Observations and interpretations of the dislocation structures. *J. geophys. Res.* **B82/36**, 5755–5770.

Frey, M. 1978. Progressive low-grade metamorphism of a black shale formation, Swiss Alps, with special reference to pyrophyllite and margarite bearing assemblages. *J. Petrology* **19**, 93–135.

Frey, M., Hunziker, J. C., Frank, W., Bocquet, J., Dal Piaz, G. V., Jaeger, E. & Niggli, E. 1974. Alpine metamorphism of the Alps: a review. *Schweiz. miner. petrogr. Mitt.* **54**, 247–290.

Frey, M. & Niggli, E. 1971. Illit-Kristallinität, Mineralfazien und Inkohlungsgrad. *Schweiz. miner. petrogr. Mitt.* **51**, 229–234.

Goetze, C. & Kohlstedt, D. L. 1977. The dislocation structure of experimentally deformed marble. *Contr. Miner. Petrol.* **59**, 293–306.

Gubler, E. 1976. Beitrag des Landesnivellements zur Bestimmung vertikaler Krustenbewegung in der Gotthard-Region. *Schweiz. miner. petrogr. Mitt.* **56**, 675–678.

Ham, R. K. 1961. Determination of dislocation densities in thin films. *Phil. Mag.* **6/69**, 1183–1184.

Heard, H. C. 1963. Effects of large changes in strain rate in the experimental deformation of Yule marble. *J. Geol.* **71**, 162–195.

Heard, H. C., & Raleigh, C. B. 1972. Steady-state flow in marble at 500C–800C. *Bull. geol. Soc. Am.* **83**, 935–956.

Hsü, K. J. 1969. A preliminary analysis of the statics and kinetics of the Glarus overthrust. *Eclog. geol. Helv.* **62**, 143–154.

Kisch, H. J. 1974. Anthracite and meta-anthracite coal ranks associated with 'anchimetamorphism' and 'very-low-stage' metamorphism. *Verh. K. ned. Akad. Wetensch. Amsterdam Ser. B* **77**, 81–118.

Milnes, A. G. & Pfiffner, O. A. 1977. Structural development of the Infrahelvetic complex, eastern Switzerland. *Eclog. geol. Helv.* **70**, 83–95.

Milnes, A. G. & Pfiffner, O. A. 1980. Tectonic evolution of the Central Alps in the cross-section St. Gallen–Como. *Eclog. geol. Helv.* **73**, 619–633.

Nicolas, A. & Poirier, J. P. 1976. *Crystalline Plasticity and Solid State Flow in Metamorphic Rocks*. Wiley, London.

Pfiffner, O. A. 1977. Tektonische Untersuchungen im Infrahelvetikum der Ostschweiz. *Mitt. geol. Inst. ETH Univ. Zürich, N.F.* **217**, 1–432.

Pfiffner, O. A. 1978. Der Falten- und Kleindeckenbau im Infrahelvetikum der Ostschweiz. *Eclog. geol. Helv.* **71**, 61–84.

Pfiffner, O. A. 1980. Strain analysis in folds (Infrahelvetic complex, Central Alps). *Tectonophysics* **61**, 337–362.

Pfiffner, O. A. 1981. Fold-and-thrust tectonics in the Helvetic nappes (E Switzerland). In: *Thrust and Nappe Tectonics* (edited by McClay, K. R. & Price, N. J.). *Spec. Publs geol. Soc. Lond.* **9**, 319–327.

Pfiffner, O. A. & Ramsay, J. G. 1982. Constraints on geological strain rates: arguments from finite strain states of naturally deformed rocks. *J. geophys. Res.* **87**, 311–321.

Rack, H. J. & Newman, R. W. 1970. Microstructures. In: *Physical Metallurgy* (edited by Cahn, R. W.). Elsevier/North-Holland, Amsterdam, 705–786.

Rutter, E. H. 1974. The influence of temperature, strain rate and interstitial water in the experimental deformation of calcite rocks. *Tectonophysics* **22**, 311–334.

Schaer, J. P. 1979. Mouvements verticaux, érosion dans les Alpes, aujourd'hui et au cours du Miocène. *Eclog. geol. Helv.* **72**, 263–270.

Schaer, J. P. & Jeanrichard, F. 1974. Mouvements verticaux anciens et actuels dans les Alpes suisses. *Eclog. geol. Helv.* **67**, 101–119.

Schmid, S. M. 1975. The Glarus overthrust: field evidence and mechanical model. *Eclog. geol. Helv.* **68**, 247–280.

Schmid, S. M. 1976. Rheological evidence for changes in the deformation mechanism of Solenhofen limestone towards low stresses. *Tectonophysics* **31**, T21–T28.

Schmid, S. M., Boland, J. N. & Paterson, M. S. 1977. Superplastic flow in finegrained limestone. *Tectonophysics* **43**, 257–291.

Schmid, S. M., Casey, M & Starkey, J. 1981. The microfabric of calcite tectonites from the Helvetic nappes (Swiss Alps). In: *Thrust and Nappe Tectonics* (edited by McClay, K. R. & Price, N. J.). *Spec. Publs geol. Soc. Lond.* **9**, 151–158.

Schmid, S. M., Paterson, M. S. & Boland, J. N. 1980. High temperature flow and dynamic recrystallization of Carrara marble. *Tectonophysics* **65**, 245–280.

Snyder, R. W. & Graff, H. F. 1938. Study of grainsize in hardened high speed metals. *Metal Prog.* (April), 377–380.

Stalder, H. A. & Touray, J. C. 1970. Fensterquarze mit Methan-Einschlüssen aus dem westlichen Teil der schweizerischen Kalkalpen. *Schweiz. miner. petrogr. Mitt.* **50**, 109–130.

Twiss, R. J. 1977. Theory and applicability of a recrystallized grain size paleopiezometer. *Pageoph.* **115**, 227–244.